THE USE OF CAVITATING JETS TO OXIDIZE ORGANIC COMPOUNDS IN WATER

K.M. Kalumuck and G.L. Chahine
Dynaflow, Inc. Jessup, MD 20794
email: info@dynaflow-inc.com

ABSTRACT

This paper reports on the application of hydrodynamic cavitation by the use of submerged cavitating liquid jets to trigger widespread cavitation and induce oxidation of organic compounds in the bulk liquid solution with a two order of magnitude increase in energy efficiency compared to the ultrasonic means.

The results are compared to a bubble dynamics model that includes heat and mass transport, collective bubble effects, and a first order Arrhenius reaction rate model. Comparison of model results with experiment indicated the reactions were limited by contaminant transport to the bubble surface rather than by radical generation or the intensity of bubble collapse. Other findings are the desirability of operating at atmospheric ambient pressure and low driving pressures and of maximizing cavity surface area. These results suggest a great potential for the use of jet cavitation in practical scale waste treatment and remediation systems.

1 Introduction

Overview

Ultrasonic cavitation is known (Brown and Goodman, 1965) to produce sonochemically activated reactions in water resulting in the formation of highly effective oxidizing hydroxyl radicals. Usually this is achieved using ultrasonic horns that send a high intensity acoustic beam into the solution and excite microcavities. Such systems have been found to promote a wide range of chemical reactions (Suslick, 1988) and to be capable of oxidizing dilute aqueous mixtures of organic compounds. However, such devices essentially self limit the efficiency of the process by achieving cavitation only in a thin layer near the surface of the sonifier and are not very efficient. We employ a mechanism for generating cavitation in a wide body of the liquid by an array of submerged cavitating jets (Chahine & Kalumuck, 2001a&b; Kalumuck & Chahine, 2000). This process can be made very efficient and also benefits from the relatively high efficiencies of pumps.

When subjected to cavitation, water undergoes dissolution according to the following chemical reaction (e.g., Suslick, 1989; Neppiras, 1980):

$$H_2O \rightarrow H^{\bullet} + OH^{\bullet}. \qquad (1)$$

The free hydroxyl radical $OH^{\bullet}$ is one of the most powerful oxidizing agents. Oxidation of organic compounds results in various intermediate and end products depending on the compound. These include water vapor, carbon dioxide, inorganic ions and short chain inorganic acids (e.g., see Suslick, 1988; Hua et al., 1995a; Skov et al., 1997). Intermediate products usually undergo subsequent oxidation. Modeling of radical production due to cavitation bubble collapse has recently been performed by Gong and Hart (1998).

A number of recent studies have used ultrasound to degrade organic contaminants. A partial list includes Hua et al. (1995a, b), Kotronarou et al. (1991), Cheung et al. (1991), and Hua and Hoffman (1996). Such work has been performed in both batch and continuous flow modes using ultrasonic horns and plates. Recently, a commercial process has employed a venturi type cavitation flow loop in combination with UV irradiation and hydrogen peroxide addition (Skov et al., 1997).

Cavitation Bubble Dynamics

It is generally accepted that water dissociates under intense insoni…cation due to the resulting growth and collapse of microscopic bubbles. The maximum pressure may be as high as $1.2 \pounds 10^4$ atm, and the temperature could be about 10,000 $^{\pm}$K (Young, 1989): Thus extremely high values of temperature and pressure are generated in a small region of space where the bubble collapse occurs. Such conditions could explain the enhancement by cavitation of the chemical dissociation of the aqueous medium releasing hydroxyl radicals.

However, cavitation bubbles rarely behave spherically. Typically, due to initial or boundary condition asymmetries and to bubble interactions, the bubble, upon collapse, forms a high speed reentering jet. In cavitating jets, elongated, rotating, and ring shaped bubble cavities form which have also been found to collapse with the formation of reentering jets (Chahine and Johnson, 1985; Chahine and Genoux, 1983).

Cavitating Water Jets

Cavitating water jet technology represents one successful attempt to harness and utilize the destructive power of cavitation. Various means and nozzle designs can be used to induce the explosive growth of microscopic cavities or bubbles within a liquid jet. Moving away from the ori…ce region, these bubbles encounter higher pressures and collapse (Chahine and Johnson, 1985; Chahine et al., 1995).

The dimensionless parameter characterizing cavitation is the cavitation number, $\sigma = \frac{P_{amb} - p_v}{\Delta P}$, where P_{amb} is the ambient liquid pressure, p_v is the liquid vapor pressure, and ΔP is the pressure drop across the nozzle. The value at which cavitation is incipient is de…ned as the cavitation inception number, σ_i: If $\sigma/\sigma_i < 1$, cavitation will occur, and as σ/σ_i decreases below unity the amount of cavitation will increase.

Figure 1: Strobe photograph of plexiglass walled swirling caivtating jet nozzle.

The swirling cavitating jet, DynaSwirl$^{\circledR}$, achieves cavitation at very high cavitation numbers (Figure 1). The ‡ow enters a swirl chamber by means of tangential injection slots. The swirl produces a central line vortex which cavitates. As the jet exits the nozzle and impacts on a wall, this …lament possesses a helicoidal shape with a vortex breakdown at the end of a rotating cork screw shape in the most unstable con…gurations. For oxidation, this jet has the additional advantage of generating a very large cavity surface area.

2 Experimental Setup

Flow Loops and Jet Nozzles

Experiments were conducted in several jet ‡ow loops and in an ultrasonic system. Investigations were also conducted in a cavitation reaction chamber constructed of plexiglass to enable viewing of the cavitation and ‡ow. Due to the potential for many organic compounds to attack plexiglass this cell was not used for actual oxidation tests. Instead, jet cavitation reactors constructed of stainless steel were utilized.

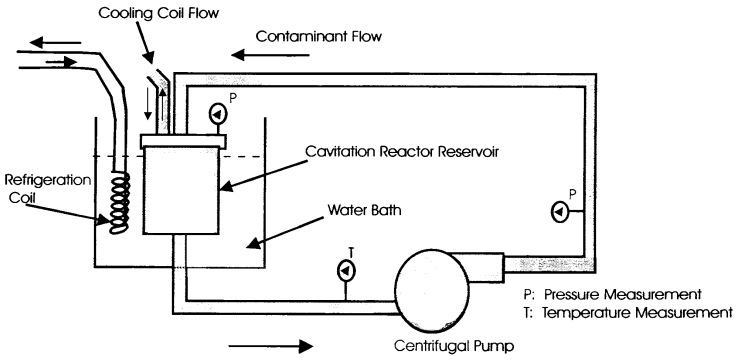

Figure 2: Sketch of flow loop

Figure 2 provides a sketch of the functional configuration of these test loops. Upon exiting the pump, the liquid flows into a cavitation reaction chamber into which various jet configurations can be inserted. The ambient pressure at the jet exit is monitored and controlled as is the pressure of the flow entering the chamber to form the jet(s). Temperature is maintained at the desired value by use of a cooling loop and tank. pH was also monitored and controlled by the addition of small quantities of phosphoric acid or sodium hydroxide. A sampling port/valve is located in the lid of the reaction chamber or in the piping exiting the chamber.

In addition to the swirling cavitating jet (Figure 1), a multi-orifice manifold configuration of StratoJet cavitating jet nozzles was employed (Kalumuck, et. al. 2000; Chahine & Johnson, 1985). The liquid flows into a pipe manifold into which a large number of orifices have been machined. The number of orifices was varied between 12 and 216. Different manifolds were utilized for different orifice diameters between 0.040 and 0.15 in. The manifold was sometimes surrounded by a cylindrical shroud onto which the jet flows were directed to enhance cavitation bubble collapse. The bubbles generated in the jet shear layer collapse in the increased pressure of the jet stagnation region along this sleeve.

To observe the cavitation characteristics and dynamics, plexiglass cavitation reaction chambers were used. The loops were operated with pure water at the same conditions as the oxidation experiments with contaminants. The results were recorded utilizing high intensity strobe lighting and a video camera with zoom lens. A series of cavitating vortex rings (Figure 3b) were distinctly visible in the jet flows in most cases.

Visualization of the swirling cavitating jet (Figure 3a) showed a large volume of cavitation in the form of a line vortex cavity that became vortical upon exiting the orifice. Typically, a cavity was seen to extend the length of the chamber along its centerline representing the cavitating core of the vortex formed by the swirling flow. As this cavity exited with the jet flow, it developed a rotating helical pattern, broke up, and collapsed.

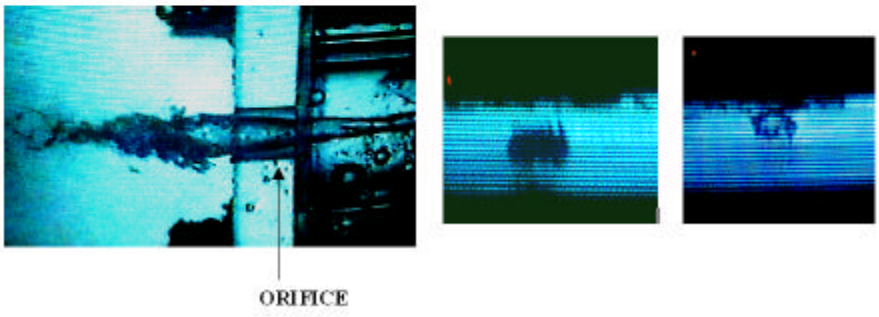

Figure 3: Visualization of cavitation generated by a) swirling jet (left) and b) multiorifice jet (center & right showing ring structures)

Measurement Techniques and Procedures

Two compounds: p-nitrophenol (PNP) and Methyl Orange (MO) were selected. PNP is a phenol related to a number of pesticides and has been studied by others using ultrasonic cavitation enabling comparison with their results. MO is an organic dye that is a nitrogen bearing aromatic compound and contains a sulphonate group, which commonly appears in detergents.

Reagent grade p-Nitrophenol PNP (Aldrich, 99%), MO, phosphoric acid (Aldrich, 85%), and sodium hydroxide (VWR Scientific, 1.0 N) were used. The PNP was in crystalline form and was mixed with distilled water. Contaminant concentrations were measured using a UV-Vis spectrophotometer following the procedures of Kotronarou et al. (1991) and Hua et al. (1995b). The spectrophotometer was calibrated against known concentrations of contaminants in distilled water. During testing, 3 ml samples were drawn from the test reservoir for concentration measurements. Detailed chemical measurement procedures can be found in Kalumuck, et. al. (2000).

3 Results and Discussion

Performance Evaluation: Oxidation Efficiency

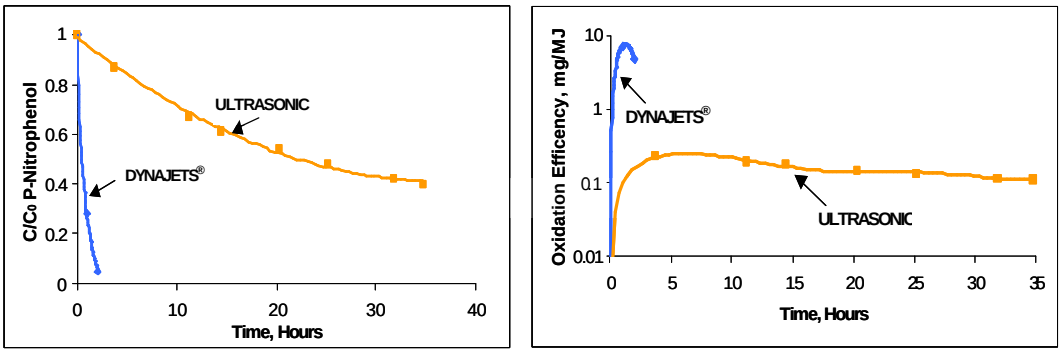

Figure 4: Comparison of concentration reduction and oxidation efficiencies of cavitating jets and ultrasonic device for PNP

A key measure of the performance of the oxidation process is the energy required to remove a unit mass of a given compound. This can be expressed as the cumulative mass of contaminant removed per unit energy expended. We define this to be the oxidation efficiency given by:

$$\eta(t) = \frac{(C_o - C(t))\,V}{\int_0^t P\,dt} \qquad (2)$$

Here, C_o is the initial concentration, $C(t)$ the concentration at time t, V the liquid volume, and P the power expended. The power used in this efficiency calculation is that which is imparted to the liquid.

Figure 4 compares the concentration reduction histories and oxidation efficiencies of jet and ultrasonic cavitation. This figure presents sample results of the oxidation of PNP (8 ppm initial concentration) with submerged cavitating jets. While the investigations conducted have not as yet been of sufficient scope to state that either the jet or ultrasonic devices are operating at their optima, a range of parameters have been investigated in the current study for the jets and in the literature for the ultrasonic device. The conditions of Figures 4 are near the best known for each device. the cavitating jet results exhibit overall energy efficiencies 100 times higher than the ultrasonic device. This suggests strong promise for application of jet cavitation to oxidation.

Cavitation Number/Ambient Pressure

Operation at elevated ambient pressures was found to be less efficient than operation of the reaction chamber at atmospheric pressure - an unexpected result as cavitation bubbles are known to collapse more strongly at elevated ambient pressures. A potential explanation is provided by the modeling effort described below

in which the temperatures of bubble collapse are predicted to be higher at the lower ambient pressures. Figure 5 presents results for ambient pressures between 24 and 100 psig and an initial PNP concentration of approximately 8 ppm with ferric sulfate addition. Both the oxidation rate and efficiency decline with increasing ambient pressure. Shown are also results for ambient pressures of 50 and 100 psig at an approximately constant value of the cavitation number, sigma ¼ 0.2. The efficiency is approximately three times greater at the lower ambient pressure. These results have very positive practical implications. There is no need to operate at elevated pressures. Thus the equipment can be relatively simple with modest capital costs.

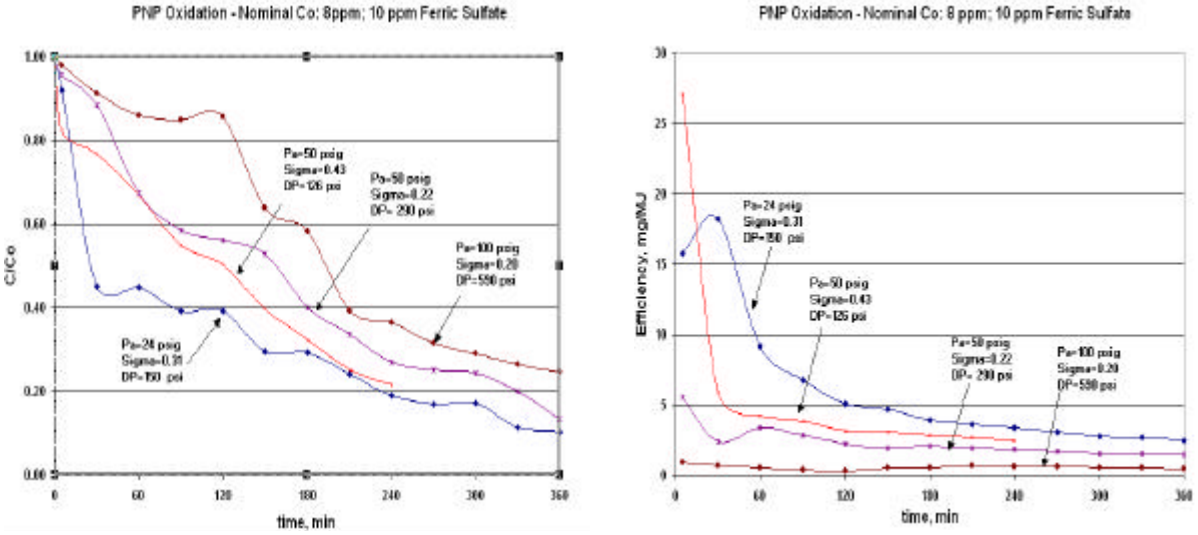

Figure 5: Influence of ambient pressure, Pa, and cavitation number, sigma, on oxidation of PNP. a) Concentration histories (left). b) Oxidation efficiencies (right).

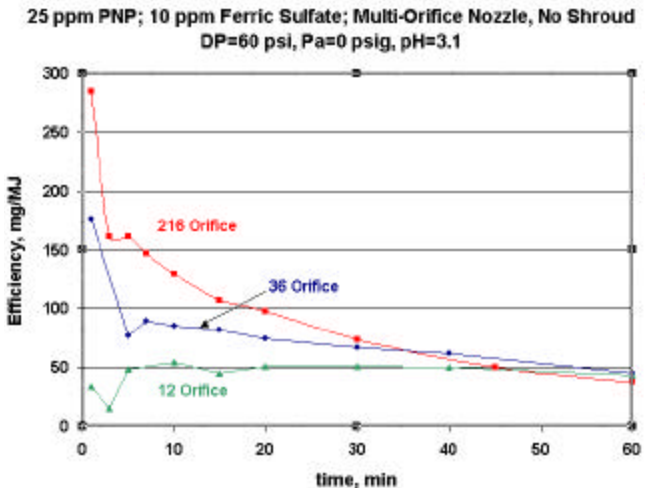

Figure 6 Influence of number and size of orifices on oxidation efficiency.

Number and Size of Orifices

Figure 6shows the influence of the number and size of the orifices for the multi-orifice manifold configuration for oxidation of PNP. Shown are the results of three different configurations: 12 orifices of 0.15 in. diameter, 36 orifices of 0.087 in. diameter and 216 orifices of 0.04 in. diameter. All were operated at the same pressures, temperature and pH. The 12 and 36 orifice cases had the same flow rate while the 216 orifice case had an increase in flow rate of 25% due to a corresponding increase in total orifice cross section area. This difference is accounted for, however, when the results are normalized by the expended power to calculate the efficiency

as done in Figure 6. The results clearly show that more smaller orifices, desirable. resulting in a increase in the total surface area of the cavities generated, is desirable.

4 Mechanistic Modeling

Conceptually, contaminant removal is a multi-step process that includes: 1) radical generation, 2) transport of contaminants and radicals, and 3) reaction between contaminant and radicals. Step 1 is presumably controlled by the bubble dynamics. Step 2 is controlled by the fluid dynamics through viscous and turbulent diffusion and mixing. Step 3 is controlled by the chemical kinetics. The models considered are briefly summarized here. More details can be found in Kalumuck, et. al. 2000.

Spherical bubble collapse model

The bubble dynamics for a bubble of radius a is modeled using a modified Rayleigh-Plesset equation that accounts for the liquid pressure change, ΔP, in the jet flow (flowing into a liquid of ambient pressure p_{amb}) and the presence of a bubble population obtained from a 1-D bubbly flow model with the liquid density dependent on the local void fraction, α:

$$\rho\left[a\frac{d^2a}{dt^2}+\frac{3}{2}\left(\frac{da}{dt}\right)^2\right]=p_g+p_v-p_{amb}-2\sigma/a-4\mu\frac{1}{a}\frac{da}{dt}=p_{g0}\left(\frac{a_0}{a}\right)^{3\gamma}\left[1-\left(\frac{\alpha}{\alpha_0}\right)^{3}\right]. \tag{3}$$

Here, σ is the surface tension, μ is the liquid viscosity, ρ the liquid density, p_g and p_v the partial pressures of noncondensible gas and vapor within the bubble. The subscript 0 refers to equilibrium conditions upstream of the jet orifice at a liquid pressure equal to $p_{amb}+\Delta P$.

The mass and thermal convection/diffusion equations in the liquid are solved using a thin boundary layer approximation (Plesset & Zwick, 1952) and Henry's Law at the liquid/cavity interface for each gas component. Vaporization/condensation occurs at the interface and latent heat is considered in the energy balance (e.g., Gumerov, 2000).

The bubble is modeled as containing an ideal gas mixture of vapor and gases. The radicals produced are taken to instantly react with contaminants near the bubble surface. Reactions are thus controlled by contaminant transport to the bubble surface and by radical generation, and no significant concentrations of contaminants or radicals are maintained within the bubble. Radical production occurs in the gaseous phase according to an exponential dependence of the rate on temperature (the commonly used Arrhenius kinetic mechanism; e.g., Perry & Green, 1984) and is proportional to the gas pressure. The reaction is modeled as 1st order with respect to the target compound concentration with a rate constant κ. We relate κ to bubble dynamics through its dependence on the bubble gas temperature and pressure:

$$\kappa=\kappa_0\left(\frac{p_g}{p_{g0}}\right)^{\nu}\exp\left(-\frac{E_{act}}{RT_g}\right);\quad T>T_{act};\quad \kappa=0;\ T<T_{act}; \tag{4}$$

where E_{act} is the activation energy, R is the universal gas constant, and ν is a constant related to the stoichiometric coefficient of reaction. This model includes a threshold dependence where T_{act} is the activation temperature. The boundary condition at the bubble interface S is:

$$\rho D\left(\frac{\partial\bar{\bar{c}}}{\partial n}\right)_S-\kappa\,\bar{\bar{c}}_S=0; \tag{5}$$

where ρ is the liquid density, c is the contaminant concentration, and D is the contaminant diffusivity in the liquid. For an initial uniform contaminant concentration, c_o, the mass flux, J, and the contaminant concentration at the bubble wall, c_a, are:

$$J=-\rho D\int_S\left(\frac{\partial\bar{\bar{c}}}{\partial n}\right)_S dS=-4\pi a^2 k c_a;\qquad c_a(t)=c_0+\frac{1}{4\pi\rho\sqrt{\pi D}}\int_0^t\frac{J(t')dt'}{\sqrt{\int_{t'}^{t}a^4(t'')dt''}}. \tag{6}$$

For a multiphase mixture of constant liquid volume V containing n bubbles, the void fraction, α, and the change in the mass m of component M are:

$$\alpha = \frac{4\pi n a^3}{3V}; \quad \frac{dm}{dt} = nJ; \quad m = c_0(1-\alpha)\rho V. \tag{7}$$

Using $\langle\cdot\rangle$ to denote the time average of a quantity and noting that $\langle J\rangle$ is a function of the initial concentration, i.e., $\langle J\rangle = F(c_0)$; the decrease of the average concentration is:

$$\frac{dc_0}{dt} = \frac{3\langle\alpha\rangle}{4\pi\rho\langle a^3\rangle(1-\langle\alpha\rangle)}\langle J\rangle = \frac{3\langle\alpha\rangle}{4\pi\rho\langle a^3\rangle(1-\langle\alpha\rangle)}F(c_0). \tag{8}$$

Equation (8) applies when the total system volume equal the volume of the cavitation chamber. For a closed loop with liquid volume V; and a cavitation zone of volume V_{cz}; the rate of oxidation for the entire volume is:

$$\frac{dc_0}{dt} = \frac{3\langle\alpha\rangle r_v}{4\pi\rho\langle a^3\rangle(1-\langle\alpha\rangle)}\langle J\rangle; \qquad r_v = \frac{V_{cz}}{V}. \tag{9}$$

The bulk contaminant concentration decrease due to the presence of many bubbles and recirculation of the liquid in the flow loop is calculated by numerically solving equations (6) and (9) in conjunction with the bubble dynamics (Kalumuck, et. al., 2000).

Results

A series of runs with varying parameters were made for conditions representative of those for the nozzle configuration with 216 orifices of 0.04 in. diameter. The baseline input data was: k_o =1000 kg/m^2; liquid diffusivity for PNP in water, $D = 2.4 \times 10^{-9}$ m^2/s; C_o =10^{-5} (10 ppm); T_{act} =5000 $^\pm$K; ^{o} =1; mean void fraction in the cavitation zone, $\langle\alpha\rangle$ = 0.02.

Figure 7 illustrates the influence of the type of noncondensible gas within the bubble: air and argon. Relative to air, argon results in a modestly increased temperature, a shorter period, and a more rapid concentration drop. At 1 hr. the air case drops to 20% of the initial concentration while the Argon case drops to about 8%. Oxidation rate increases due to the presence of an inert gas such as Argon are repeatedly reported in the literature for ultrasonic oxidation. However, our jet experiments showed no significant effects due to the addition of Argon.

Figure 8 shows the influence of ambient pressure at a constant cavitation number of 0.25. Since the cavitation number is conserved, the jet velocity is higher in the elevated ambient pressure case resulting in less transit time before impingement on the plate. The lower ambient pressure case results in higher temperatures and more rapid oxidation. This is also found experimentally. The power required to operate at twice the pressure (and thus 40% more flow) is 2.8 times as large. Thus, for 1 hr of operation, the lower pressure case efficiency is greater by a factor of 3.4.

Infinite Reaction Rate Limiting Case Models

A limiting case is when the reaction rate is fast enough and the reactants sufficiently abundant that any molecule of contaminant reaching the bubble surface will instantly disappear though a reaction. The reaction rate is thus limited by contaminant transport to the bubble surface and the total bubble surface area. This represents an upper limit on how rapidly a contaminant can disappear. For spherical, toroidal, and cylindrical bubble shapes, solution of eq. (9) for the contaminant concentration, C, with initial value C_o, exhibits an exponential decrease with time, t; (as shown below):

$$C = C_o e^{-\gamma t}; \qquad \gamma = B\frac{S_{max}}{V}\sqrt{\frac{D}{T_{cz}}}; \quad T_{cz} = \frac{V_{cz}}{Q}. \tag{10}$$

Here, S_{max} is the maximum bubble surface area, V is the total flow loop liquid volume, V_{cz} is the liquid volume in the cavitation zone, Q is the volumetric flow rate through the loop, and D is the diffusivity of the contaminant in the liquid. The time scale T_{cz} is the liquid mean residence time in the cavitation zone. B is a constant that depends on the specific bubble geometry.

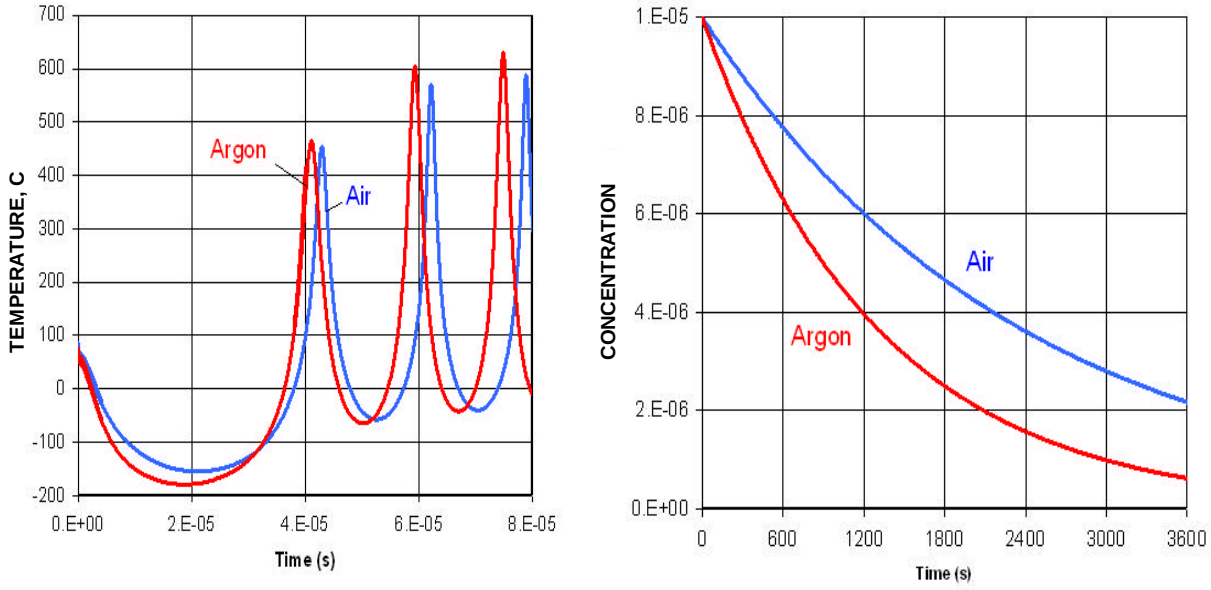

Figure 7: Calculated influence of type of noncondensible gas (air and Argon) within bubble on oxidation of PNP. Left: temperature within bubble. Right: Concentration history.

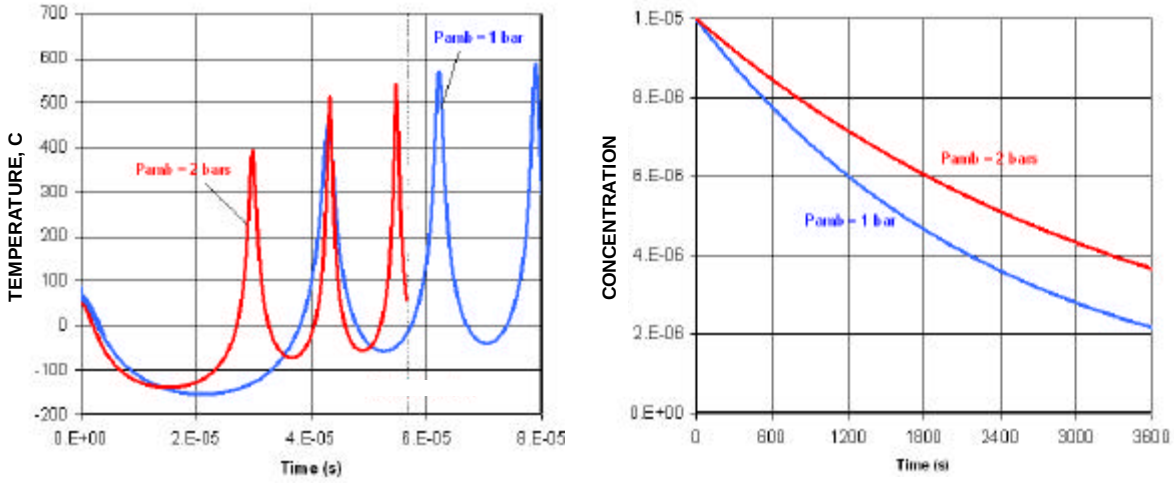

Figure 8: Computed bubble dynamics in the flow field of a submerged jet with mass and heat transfer: influence of ambient pressure on bubble temperature history and oxidation of contaminant. Cavitation Number = 0.25, ambient temperature = 50 °C, initial bubble size = 0.1 mm.

Spherical Bubble

For a single spherical bubble, expression (6) for mass flux becomes:

$$J = -\rho D \int_S \frac{\partial c}{\partial n}\bigg|_S dS = -4\pi\rho_0 a^4 \frac{D}{\mathcal{R}_t \int_0^t a^4(t')dt'}. \qquad (11)$$

For a multiphase medium,

$$\langle J \rangle = -8\pi^{1/2} c_0 \sqrt{\frac{D}{\pi T}} \langle a^4 \rangle . \tag{12}$$

We find that expression (9) simplifies for $\langle \alpha \rangle \ll 0$ (small void fraction) to (10) with

$$B = \frac{2}{\sqrt{\pi}}; \quad S_{max} = 4\pi n a_{max}^2 . \tag{13}$$

We evaluated these expressions and compared with experimental data for PNP oxidation using the 216 1-mm orifice nozzle ($\Delta P = 60$ psi, $P_{amb} = 1$ atm, $Q = 5.4$ gpm, $V = 7.9$ liters, $r_v = 0.0003$, $D = 2.4 \times 10^{-9}$ m^2/s; $T_{loop} = 2.3$ s). The value of the decay constant was found to be: $0.09 < \beta < 0.024$ min^{-1}. This was calculated from the measured concentrations over the time period needed for a factor of ten reduction in concentration (which varied between 25 and 95 min.) We set $n = 216 n^*$; where n^* is the average number of bubbles, of maximum radius a_{max}, simultaneously present for each of the 216 nozzles. Using these values in expressions (10) and (13), the calculated values of β are found to be within this experimental range for $n^* = 2$, 3, and 4 when $a_{max} = 0.5$ mm (the orifice radius) and for $n^* = 1$ and 2 when $a_{max} = 1$ mm (twice the orifice radius).

Toroidal Bubble

If the cavities are considered to be toroids with major diameter, D_{ring}, and minor (cross-sectional) diameter, d_{ring}, the surface area S is given by:

$$S = \pi^2 D_{ring}^2 \frac{d_{ring}}{D_{ring}}; \tag{14}$$

and B remains the same as in (13). From observation, D_{ring} is of the order of 1 to 2 times the orifice diameter, and thus 0.1 to 0.2 cm for the cases considered. Results of evaluation of relation (10) that yield predicted values of β within the measured range for values of n^* of 3 or less (consistent with observations) show that the ratio d_{ring}/D_{ring} should be in the range 0.2 - 0.3. The presence of 1 to 3 rings is typical in the experiments as are these values of D_{ring}; and d_{ring}/D_{ring}.

The above analysis and evaluations suggest that, at least within the parameter range of the listed experiments, the jet oxidation process may be controlled by transport of contaminants to cavity surfaces and be relatively insensitive to radical generation rate and the rate of the kinetics of the oxidation reaction.

Oxidation in a Swirl Flow with a Gaseous Core

We derived a limiting case expression for diffusion to a central line vortex cavity to model contaminant transport to the cavity in the swirl chamber of the swirling cavitating jet. The reaction is considered to take place immediately as the contaminant reaches the cavity surface. We model the swirling jet flow as steady and axisymmetric about a central gaseous modeled as an infinite cylinder of constant radius a: We consider a uniform angular (tangential) flow velocity near the cylinder and an axial flow parallel to the cylinder and assume that these components of the velocity depend only on the radial distance r. The transport of a dissolved compound of concentration c to the cylindrical core can be described by the convection-diffusion equation. For the limiting case of infinite reaction rate and for a thin diffusion boundary layer, we find:

$$c = c_1 \operatorname{erf}\left(\frac{r - a}{2} \sqrt{\frac{U}{Dz}} \right); \qquad J = -2\pi c_1 a \sqrt{lDU}; \tag{15}$$

where R is the radius of the boundary of the swirl chamber, l is the cavity length, U the average axial velocity computed from the flow rate and the cross sectional area of the swirl chamber, and z is the axial distance from the upstream end of the cavity. We find that (10) again applies with:

$$S_{max} = 2\pi a L_{sc}; \quad B = 1; \quad V_{cz} = V_{sc}; \tag{16}$$

where V_{sc} is the swirl chamber volume, and L_{sc} is the swirl chamber length - or total cavity length within the chamber.

The values of ¸ were evaluated for various swirling jet cases for 1 hour of operation ($D = 2.4 \times 10^{-5}$ cm^2/s, V = 8 liters, a ¼ 0.25 cm) and are plotted versus the flow rate in Figure 9. The data have been fit with a power relation that provides a best-fit value of 0.5 for the power of Q. The predicted values are low by a factor of 5 to 10 relative to the data. This may be due to contaminant transport mechanisms, such as bulk transport due to recirculation and turbulent transport, not considered in the model. The value of D used in evaluating expression (10) was the laminar flow molecular diffusivity equal to 2.4×10^{-5} cm^2/s which we define as D_o. If D is replaced with a turbulent diffusivity 33 times the molecular value, the predictions match the "best fit" power relation of the data. This is not an unreasonable value for turbulent diffusivity.

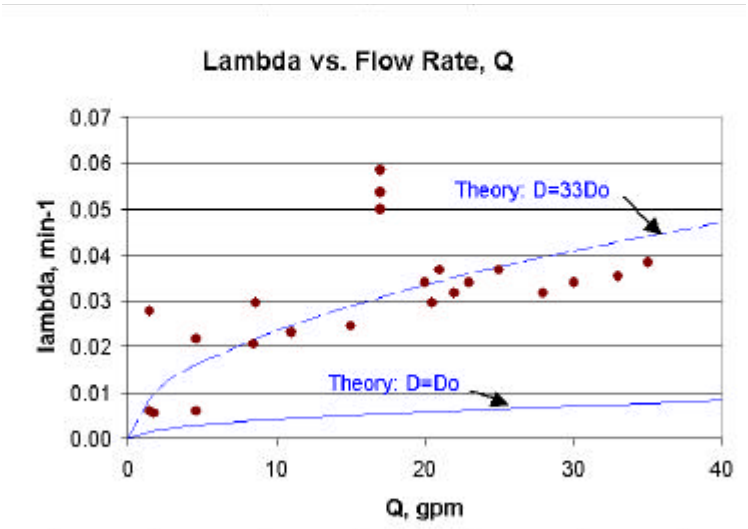

Figure 9: Comparison of measured and computed concentration decay constants, lambda, for swirling cavitating jet oxidation of Methyl Orange for 60 min. of operation. $D_o = 2.4 \times 10^{-5}$ cm^2/s, the laminar flow diffusivity.

5 Summary & Conclusions

Experiments and modeling on the use of jet induced cavitation to oxidize dilute aqueous solutions of organic compounds were performed. Experiments with p-Nitrophenol and Methyl Orange demonstrated the ability of these jets to rapidly reduce the concentrations of both compounds below 1 ppm (the lowest value we could accurately measure with our instrumentation) and to do so with more that a two order of magnitude increase in energy efficiency compared to an ultrasonic device.

Additional findings include:

- Highest efficiencies were obtained with the lowest flow rates and pressures.
- The efficiency increases with increase in the total cavity surface area due to a large number of small orifices.
- Analysis indicated the reactions were limited by contaminant transport to bubble surfaces.
- Operation at elevated ambient pressures was not found to result in more rapid oxidation. Thus from an efficiency standpoint, it is desirable to operate near atmospheric ambient pressure. This is unanticipated in that it is well known that higher ambient pressures produce more intense bubble collapse. A potential explanation is that the jet cavitation collapse at atmospheric pressure produces sufficient radicals such that an increase in intensity does not change the oxidation rates.

Acknowledgments

The authors wish to thank Dr. Nail Gumerov of Dynaflow for discussions and modeling efforts and Dr. Lawrence Principe of Johns Hopkins University for a number of helpful discussions and consultations. This work was sponsored in part by NSF under SBIR award No. DMI-9 661572.

References

Brown, B. and Goodman, J. E., 1965, High Intensity Ultrasonics, Van Nostrand Inc., Princeton, NJ.

Chahine, G.L. and Genoux, Ph., 1983, "Collapse of a Cavitating Vortex Ring," Journal of Fluids Engineering, Vol. 105, pp. 400-405.

Chahine G.L., and Johnson V.E.. Jr., 1985, "Mechanics and Applications of Self-Resonating Cavitating Jets," International Symposium on Jets and Cavities, ASME, WAM, Miami, FL.

Chahine, G.L. & Kalumuck, K.M., 2001a, "Fluid Jet Cavitation Method and System for Efficient Decontamination of Liquids," U.S. Patent No. 6,200,486.

Chahine, G.L. & Kalumuck, K.M., 2001b "Swirling Fluid Jet Cavitation Method and System for Efficient Decontamination of Liquids," U.S. Patent No. 6,221,260.

Chahine, G.L., Kalumuck, K.M., & Frederick, G.S., 1995, "Cavitating Water Jets for Deep Hole Drilling in Hard Rock," Proc., 8th American Water Jet Conference, Houston, TX, Vol. 2, pp. 765-778.

Cheung, H.M., Bhatnagar, A. and Jansen, G., 1991, "Sonochemical Destruction of Chlorinated Hydrocarbons in Dilute Aqueous Solution," Env. Sci. & Techn., Vol. 25, pp. 1510.

Genoux, Ph. and Chahine, G.L., 1984, "Simulation of the Pressure Field Due to a Submerged Oscillating Jet Impacting on a Solid Wall," Journal of Fluids Engineering, Vol. 106, pp. 491-496.

Gong, C. and Hart, D.P., 1998, "Ultrasound Induced Cavitation and Sonochemical Yields," Journal of the Acoustical Society of America, vol. 104, No. 4, pp. 2675-2682.

Gumerov, N.A., 2000, "Dynamics of Vapor Bubbles with Non-Equilibrium Phase transitions in Isotropic Acoustic Fields," Physics of Fluids, vol 12, No. 1.

Hua, I., Hochemer, R., and Hoffman, M., 1995a, "Sonochenmical Degradation of p-Nitrophenol in a Parallel Plate Near Field Acoustic Processor," Env. Sci. & Techn., Vol. 29, pp. 2790-2796.

Hua, I., Hochemer, R., and Hoffman, M., 1995b, "Sonolytic Hydrolysis of p-Nitrophenyl Acetate: The Role of Supercritical Water," Journal of Physical Chemistry, Vol. 99, pp. 2335-2342.

Hua, I. and Hoffman, M., 1996, "Kinetics and Mechanism of the Sonolytic Degradation of CCl_4: Intermediates and Byproducts," Env. Sci. & Techn., Vol. 30, pp. 864-871.

Kalumuck, K.M. & Chahine, G.L., 2000, "The Use of Cavitating Jets to Oxidize Organic Compounds in Water," Journal of Fluids Engineering, Vol. 122, pp.465-470. (Also in Proceedings, ASME Fluids Engineering Summer Meeting, Washington D.C., ASME FEDSM 98-4813, June 1998.)

Kalumuck, K.M., Chahine, G.L., Gumerov, N.A., Aley, P.D., & Frederick, G.S., 2000, "Oxidation of Organic Compounds in Water with Cavitating Jets - Phase II" Dynaflow, Inc. Tech. Rpt. 98010.

Kotronarou, A., Mills, G., and Hoffman, M., 1991, "Ultrasonic Irradiation of p-Nitrophenol in Aqueous Solution," Journal of Physical Chemistry, Vol. 95, pp. 3630-3638.

Neppiras, E.A., 1980, "Acoustic Cavitation," Phys. Rep., 61, 159-251.

Perry, R. & Green, D., eds., 1984, Perry's Chemical Engineers' Handbook, 6th ed., McGraw-Hill, NY.

Plesset, M.S. and Zwick, S.A., 1952, "An Onsteady Heat Diffusion Problem with Spherical Symmetry," J. Applied Physics, vol. 23, No. 1.

Skov, E., Pisani, J. and Beale, S., 1997, "Cavitation Induced Hydroxyl Radical Formation," American Institute of Chemical Engineering National Meeting, Houston,TX.

Suslick, K.S., ed., 1988, Ultrasound, Its Chemical, Physical, and Biological Effects, VCH, New York.

Suslick, K.S., Cline, Jr., R.E., and Hammerton, D..A., 1986, "The Sonochemical Hot Spot," Journal of the American Chemical Society, Vol. 108, p. 5641.

Suslick, K.S., 1989, "Sonochemistry," Science, Vol. 247, pp. 1439-1445.

Young, F.R., 1989, Cavitation, McGraw-Hill, London.